

Electronic transport in graphene-based heterostructures

J. Y. Tan^{1,2}, A. Avsar^{1,2}, J. Balakrishnan^{1,2}, G. K.W. Koon^{1,2,3}, T. Taychatanapat^{1,2}, E. C. T. O'Farrell^{1,2}, K. Watanabe⁴, T. Taniguchi⁴, G. Eda^{1,2}, A. H. Castro Neto^{1,2}, and B. Özyilmaz^{1,2,3,a)}

¹Graphene Research Center, National University of Singapore, 117542, Singapore, ²Department of Physics, National University of Singapore, 117542, Singapore, ³NanoCore, National University of Singapore, 117576, Singapore, ⁴National Institute for Materials Science, 1-1 Namiki, Tsukuba 305-0044, Japan

While boron nitride (BN) substrates have been utilized to achieve high electronic mobilities in graphene field effect transistors, it is unclear how other layered two dimensional (2D) crystals influence the electronic performance of graphene. In this letter, we study the surface morphology of 2D BN, gallium selenide (GaSe), and transition metal dichalcogenides (tungsten disulfide (WS₂) and molybdenum disulfide (MoS₂)) crystals and their influence on graphene's electronic quality. Atomic force microscopy analysis show that these crystals have improved surface roughness (root mean square (rms) value of only $\sim 0.1\text{nm}$) compared to conventional SiO₂ substrate. While our results confirm that graphene devices exhibit very high electronic mobility (μ) on BN substrates, graphene devices on WS₂ substrates (G/WS₂) are equally promising for high quality electronic transport ($\mu\sim 38,000\text{ cm}^2/\text{Vs}$ at RT), followed by G/MoS₂ ($\mu\sim 10,000\text{ cm}^2/\text{Vs}$) and G/GaSe ($\mu\sim 2,200\text{ cm}^2/\text{Vs}$). However, we observe a significant asymmetry in electron and hole conduction in G/WS₂ and G/MoS₂ heterostructures, most likely due to the presence of sulphur vacancies in the substrate crystals. GaSe crystals are observed to degrade over time even under ambient conditions, leading to a large hysteresis in graphene transport making it a less suitable substrate.

^{a)} Author to whom correspondence should be addressed. Electronic mail: barbaros@nus.edu.sg

Isolated new 2D materials beyond graphene such as WS₂, MoS₂, and GaSe exhibit many exotic electronic¹, optical²⁻⁴, spintronics⁵ and mechanical⁶ properties. Recent development in the transfer of these ultra thin planar structures onto each other with precise control offers outstanding opportunities for fundamental and applied studies. For example, the replacement of common silicon dioxide (SiO₂) substrate with ultra flat BN crystal resulted in a significant enhancement in electronic mobility of graphene that allowed the observation of room temperature (RT) ballistic transport⁷⁻⁸ and fractional quantum Hall effect⁹. Combination of graphene with BN, WS₂ and MoS₂ crystals also enabled new memory and transistor concepts¹⁰⁻¹¹. Recently, graphene and WS₂-based heterostructures have been demonstrated in highly flexible photovoltaic devices with extremely high external quantum efficiency¹². Graphene based heterostructure devices built with MoS₂ or GaSe are also expected to exhibit similar behavior. Last but not least important, WS₂ was proposed to enhance the weak spin orbit coupling of graphene with a proximity effect¹³. Since graphene and these 2D crystals are the most active elements in current and possibly future heterostructure devices, it is important to understand the impact of these crystals on the electronic quality of graphene before building increasingly complex heterostructures.

In this letter, we study the electronic quality of graphene on various substrates. While WS₂ and MoS₂ have similar chemical and structural properties, G/WS₂ heterostructures exhibit four-fold higher electronic mobility than that of G/MoS₂, making WS₂ an attractive alternative to BN substrates. We observe conductivity saturation on electron side above a threshold voltage in G/WS₂ devices. GaSe crystals are found to be less inert to ambient conditions and graphene devices fabricated on GaSe crystals exhibit even lower mobilities than the graphene devices on

SiO₂ substrates. Our results demonstrate the importance of ideal choice of material for graphene-based heterostructure devices.

To study the surface morphology of crystals, micromechanical exfoliation method is employed to deposit relatively thick crystals of BN¹⁴, WS₂¹⁵, MoS₂ (Structure Probe Inc.-SPI, natural molybenite) and GaSe (HQ Graphene) on Si/SiO₂ wafers. Dark field imaging technique is implemented to select the potential candidate flakes of a ~300 μm² clean surface area and a height of ~20nm. Fig.1. (a-c) show the typical AFM images of BN, WS₂, and MoS₂ flakes after annealing in Ar/H₂ (9/1) gaseous mixture at 400°C for 6 hours to remove possible tape residues. We noticed that unlike other crystals, GaSe crystals corrode even under ambient conditions and corrode faster if the flakes are annealed or kept under strong intensity of light. The AFM images of GaSe flakes immediately after exfoliation and 1 day after exfoliation without annealing are shown in Fig. 1(d) and (e) respectively. The height histograms of the crystals are shown in Fig.1. (g) and corresponding rms roughness of corresponding crystals are summarized in Fig.1.(h). Fig.1. (f) is the AFM image of a conventional SiO₂ substrate for comparison purpose. BN has the flattest surface (~0.06nm) followed by WS₂ (~0.08nm), MoS₂ (~0.09nm), fresh GaSe (~0.12nm), and SiO₂ (~0.17nm). The roughness of a GaSe crystal increases from 0.12 nm to 0.185 nm after only one day even though the sample was kept in high vacuum, becoming rougher than SiO₂. Since the work functions of these 2D materials and graphene are similar, the charge neutrality point (CNP) of graphene is expected to be located at the center of band gap of these crystals, making them viable alternative substrate to SiO₂ for graphene field effect transistors¹⁶.

The fabrication of graphene based heterostructure devices starts with micromechanical exfoliation of a graphene flake on a bilayer polymer stack adapted from Ref. 7. The bottom layer

of the polymer stack is dissolved to isolate the remaining resist and the graphene from the supporting substrate. The resulting film is transferred onto previously exfoliated crystals. During this procedure, the graphene surface to be transferred onto the crystal surface never gets exposed to any solvent, resulting in ultra clean interfaces. Similar to previous reports on G/BN heterostructures¹⁷⁻¹⁸, we observe bubble formation also at the interfaces of G/WS₂ and G/MoS₂ heterostructures. In order to minimize the effect of GaSe crystal degradation onto the electronic quality of graphene, graphene is transferred on GaSe immediately after it is characterized under optical microscope. Graphene is patterned with e-beam lithography into Hall bar structures in flat, bubble and wrinkle free regions and etched by O₂ plasma. The width and length of the graphene channels are 1 μm and 3 μm respectively. Finally Cr/Au (2 nm/100 nm) contacts are formed by thermal evaporation under high vacuum conditions. The devices are annealed at 340°C for 6 hours under Ar/H₂ gaseous mixture to minimize fabrication residues after etching and contact fabrication processes. Different from the rest, graphene on GaSe samples are fabricated without annealing. The optical image of a completed graphene device on WS₂ substrate is shown in Fig.1. (i). Transport measurements are performed with a four terminal ac lock-in technique under vacuum environment.

Compared to graphene on a SiO₂ substrate, graphene on a BN substrate has been already shown to have smaller impurity doping level and higher charge mobilities which is attributed to reduced surface roughness and surface charge traps¹⁹⁻²⁰. We first performed charge characterization of a graphene device on BN substrate. Fig.2.(a) inset shows the back gate voltage (V_{BG}) dependence of the graphene resistivity (ρ) as determined from $\rho = \frac{RW}{l}$ where w is the width of graphene channel and l is the spacing between electrodes. Charge neutrality point (CNP) is observed to be almost at $V_{BG} \sim 0$, resistivity is below 50 Ω at the charge carrier density

of $2 \times 10^{11} \text{cm}^{-2}$ and full width at half maximum is extremely small ($\sim 0.5 \text{V}$) indicating that the sample has very high charge mobility. At the low density regime, a field effect mobility of $\sim 300,000 \text{ cm}^2/\text{Vs}$ ($\sim 190,000 \text{ cm}^2/\text{Vs}$) at 5K (300K) is extracted using $\mu = \frac{1}{e} \frac{d\sigma}{dn}$. This is consistent with the values previously reported.^{7-8,19-20}

Next, we present the resistivity and conductivity of graphene on WS_2 substrate as a function of V_{BG} at RT (Fig.2-a). Several features immediately distinguish the transport of this device from those on usual insulating substrates such as SiO_2 . We observe that the conductivity is remarkably linear in V_{BG} on hole side, however the sample exhibits a V_{BG} independent conductivity above $V_{\text{BG}} \sim 45 \text{V}$ on electron side. While reaching to the conduction channel of WS_2 could raise similar phenomena in graphene transport, the recent observation of hopping type transport in transition metal dichalcogenides due to the presence of high concentration of sulphur vacancies²¹ suggests that these defect induced localized states act as a sink to the electronic charges of graphene once the Fermi level aligns with the level of localized states. For mobility discussion, we limit our analysis to the hole doped region. RT (6K) hole carrier mobilities of $\sim 38,000$ ($46,000$) cm^2/Vs at $5 \times 10^{11} \text{cm}^{-2}$ and $\sim 28,000$ ($30,500$) cm^2/Vs at $3 \times 10^{12} \text{cm}^{-2}$ are extracted. By using $\sigma^{-1} = ((ne\mu) + \sigma_0)^{-1} + \rho_s$, a density independent RT mobility of $35,000 \text{ cm}^2/\text{Vs}$ is calculated. Electronic mobility of graphene on WS_2 is four times higher than on SiO_2 substrate and this makes WS_2 an appealing substrate for graphene to reach high mobilities. Even though we consistently get high mobilities, the position of the CNP is sample dependent. For the present sample, the CNP is located at $V_{\text{BG}} \sim 14 \text{V}$.

As a next step, we characterize the electronic quality of graphene on a MoS_2 substrate at RT. In all measured MoS_2 devices, we observe very high asymmetry in between electron and

hole conductivity at RT (Fig.2.(b)). However, the electron conductivity of graphene on MoS₂ is not saturated within the V_{BG} range applied. For the present device, a hole mobility of ~ 10,000 cm²/Vs and an electron mobility of ~ 1,100 cm²/V.s are calculated away from CNP. The sheet resistance in hole conduction side is ~250Ω which is higher than the value obtained for BN and WS₂ based graphene devices, but still comparable to the one on SiO₂ substrate⁹. A weak electron doping, possibly resulting from the impurities in MoS₂, is observed in the shown device²².

While the surface roughness for MoS₂ and WS₂ are comparable, graphene on MoS₂ substrate has lower mobilities when compared to WS₂. We attribute this discrepancy to the lower thermal stability of MoS₂ leading to charge scattering from the oxidized MoS₂ surface. MoS₂ oxidation is reported to occur below 100 C in ambient conditions²³. As mentioned previously, graphene based heterostructures are annealed several times at 340 C under gaseous mixture to remove the fabrication residues. We believe this annealing process results in the oxidation of the MoS₂ substrate and limiting the electronic performance of graphene on MoS₂. However the WS₂ surface is less prone to such oxidation compared to MoS₂ thus thermal annealing is more effective for achieving high mobilities on WS₂ samples^{24,25}. For G/MoS₂ devices, instead of cleaning by annealing, mechanical cleaning can be adopted to improve the electronic quality of graphene while preventing the oxidation of the surface²⁶.

Finally, we measured graphene resistivity as a function of V_{BG} on GaSe at 5 K (Fig 3-(a)). A field effect mobility of ~ 2,200 cm²/Vs is extracted for the shown sample. The CNP of graphene is observed to be highly doped (V_{BG} = 32 V). Similar low quality transport was observed in ultra flat graphene device on mica substrate and associated to the presence of charge traps on substrate²⁷⁻²⁸. In order to check the effect of GaSe charge traps onto the charge transport properties of graphene, we record the resistance while the V_{BG} is swept forward (negative to

positive) and backward (positive to negative) scans (Fig 3 (b)). We observe a significant hysteresis in resistivity and the hysteresis increases as V_{BG} range increases. For example the hysteresis at a 50 V range is only ~ 2 V and it increases to ~ 37 V as the range increases to 90 V. The density of charge traps can be calculated by, $n_{tr} = C_g \Delta V / e$, where ΔV is the shift of the CNP with forward and backward sweeps, C_g is the effective capacitance, $\sim 718.5 \text{ e}(\mu\text{m})^{-2}\text{V}^{-1}$, and e is the charge²⁹. We calculated a charge trap density of $1.45 \times 10^{11} \text{ cm}^{-2}$ for $V_{BG}=50$ V range and $2.6 \times 10^{12} \text{ cm}^{-2}$ for 90 V range. The observed hysteresis in our system still persists even when the sample 1-) was measured at liquid helium temperatures. 2-) had undergone in-situ vacuum treatment at 1.5×10^{-6} Torr for 72 hours, 3-) was in-situ annealed at 100°C for 6 hours under high vacuum conditions and 4-) post annealed at 340°C with a Ar/H₂ gaseous mixture in furnace. These observations exclude the water as a source of hysteresis²⁹⁻³⁰. As confirmed by our AFM characterization and recently discussed in a review by A. K. Geim et al¹³, 2D GaSe flakes are not stable at ambient conditions and possibly creating the observed high density charged traps. Figure 3. (c) shows the dark field images of GaSe crystal just after exfoliation and 20, 40 and 80 seconds after capturing the first image. This degradation in ambient conditions is responsible for the observed high concentration of charged traps and this limits the electronic quality of graphene.

In summary, we have showed that 2D crystals have flatter surfaces than conventional SiO₂ substrates. Similar to previous reported values, we obtain very high electronic mobilities in G/BN heterostructures, followed by WS₂, MoS₂, and GaSe. Even though WS₂ has similar surface morphology with MoS₂, we observe higher mobilities in graphene devices on WS₂ than MoS₂. The observation of high density of charge traps on GaSe surface results in low mobility

graphene. Our results demonstrate that the transport properties of graphene strongly depend on the underlying substrate and address the importance of choosing appropriately the active 2D crystals for heterostructure devices.

Note added in proof: During the preparation of this manuscript, we became aware of related works on the electronic transport in graphene-based heterostructures.^{31,32}

B. Ö. would like to acknowledge support by the National Research Foundation, Prime Minister's Office, Singapore under its Research Fellowship (RF Award No. NRF-RF2008-7), and the SMF-NUS Research Horizons Award 2009-Phase II. A.H.C.N. would like to acknowledge support by the National Research Foundation, Prime Minister's Office, Singapore under its Competitive Research Programme (CRP Award No. NRF-CRP6-2010-5). G.E acknowledges Singapore National Research Foundation for funding the research under NRF Research Fellowship (NRF-NRFF2011-02).

References

- ¹ Q. H. Wang, K. Kalantar-Zadeh, A. Kis, J. N. Coleman, and M. S. Strano, *Nature Nanotechnol.* **7**, 699-712 (2012).
- ² W. J. Yu, Y. Liu, H. Zhou, A. Yin, Z. Li, Y. Huang, and X. Duan, *Nature Nanotechnol.* doi:10.1038/nnano.2013.219 (2013).
- ³ K. Roy, M. Padmanabhan, S. Goswami, T. P. Sai, G. Ramalingam, S. Raghavan, and A. Ghosh, *Nature Nanotechnol.* **8**, 826-830 (2013).
- ⁴ P. Hu, Z. Wen, L. Wang, P. Tan, and K. Xiao, *Nano Lett.* **6**, 7 (2012).
- ⁵ H. Yuan, M. S. Bahramy, K. Morimoto, S. Wu, K. Nomura, B. J. Yang, H. Shimotani, R. Suzuki, M. Toh, C. Kloc, X. Xu, R. Arita, N. Nagaosa, and Y. Iwasa, *Nature Phys.* **9**, 563-569 (2013).
- ⁶ K. S. Novoselov, and A. H. Castro Neto, *Phys. Scr.* **2012**, 014006 (2012).
- ⁷ A. S. Mayorov, R. V. Gorbachev, S. V. Morozov, L. Britnell, R. Jalil, L. A. Ponomarenko, P. Blake, K. S. Novoselov, K. Watanabe, T. Taniguchi, and A. K. Geim, *Nano Lett.* **11**, 2396-2399 (2011).
- ⁸ L. Wang, I. Meric, P. Y. Huang, Q. Gao, Y. Gao, H. Tran, T. Taniguchi, K. Watanabe, L. M. Campos, D. A. Muller, J. Guo, P. Kim, J. Hone, K. L. Shepard, and C. R. Dean, *Science*, **342**, 614-617 (2013).
- ⁹ C. R. Dean, A. F. Young, P. C. Zimansky, L. Wang, H. Ren, K. Watanabe, T. Taniguchi, P. Kim, J. Hone, and K. L. Shepard, *Nature Phys.* **7**, 693 (2011).
- ¹⁰ M. S. Choi, G.-H. Lee, Y.-J. Yu, D.-Y Lee, S. H. Lee, P. Kim, J. Hone, and W. J. Yoo, *Nature Comm.* **4**, 1624 (2013).

- 11 L. Britnell, R. V. Gorbachev, R. Jalil, B. D. Belle, F. Schedin, A. Mishchenko, T. Georgiou, L. Eaves, S. V. Morozov, N. M. R. Peres, J. Leist, A. K. Geim, K. S. Novoselov, and L. A. Ponomarenko, *Science*, **335**, 947-950 (2012).
- 12 L. Britnell, R. M. Ribeiro, A. Eckmann, R. Jalil, B. D. Belle, A. Mishchenko, Y.-J. Kim, R. V. Gorbachev, T. Georgiou, S. V. Morozov, A. N. Grigorenko, A. K. Geim, C. Casiraghi, A. H. Castro Neto, and K. S. Novoselov, *Science*, **340**, 1311-1314 (2013).
- 13 A. K. Geim, and I. V. Grigorieva, *Nature*, **499**, 419 (2013).
- 14 T. Taniguchi, and K. Watanabe, *J. Cryst. Growth* **303**, 525-529 (2007).
- 15 W. Zhao, Z. Ghorannevis, L. Chu, M. L. Toh, C. Kloc, P.-H. Tan, and G. Eda, *ACS Nano*, **7**, 791 (2013).
- 16 C. Gong, H. Zhang, W. Wang, L. Colombo, R. M. Wallace, and K. Cho, *Appl. Phys. Lett.* **103**, 052513 (2013).
- 17 W. Pan, J. Xiao, J. Zhu, C. Yu, G. Zhang, Z. Ni, K. Watanabe, T. Taniguchi, Y. Shi, and X. Wang, *Scientific Reports*, **2**, 893 (2012).
- 18 S. J. Haigh, A. Gholinia, R. Jalil, S. Romani, L. Britnell, D. C. Elias, K. S. Novoselov, L. A. Ponomarenko, A. K. Geim, and R. Gorbachev, *Nature Materials*, **11**, 764-767 (2012).
- 19 C. R. Dean, A. F. Young, I. Meric, C. Lee, L. Wang, S. Sorgenfrei, K. Watanabe, T. Taniguchi, P. Kim, K. L. Shepard, and J. Hone, *Nat. Nanotechnol.* **5**, 722 (2010).
- 20 P. J. Zomer, S. P. Dash, N. Tombros, and B. J. van Wees, *Appl. Phys. Lett.* **99**, 232104 (2011).
- 21 H. Qiu, T. Xu, Z. Wang, W. Ren, H. Nan, Z. Ni, Q. Chen, S. Yuan, F. Miao, F. Song, G. Long, Y. Shi, L. Sun, J. Wang, and X. Wang, *Nature Comm.*, **4**, 2642 (2013).

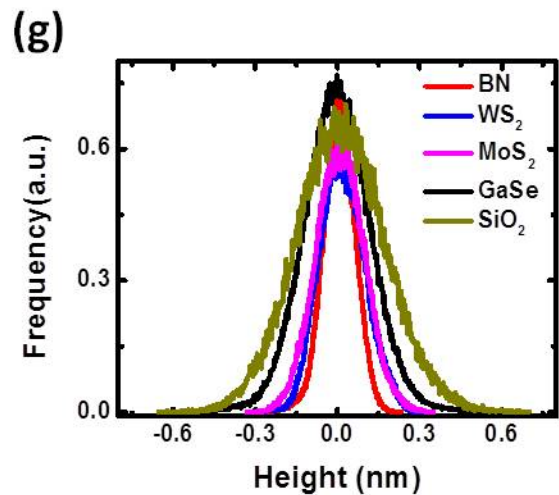
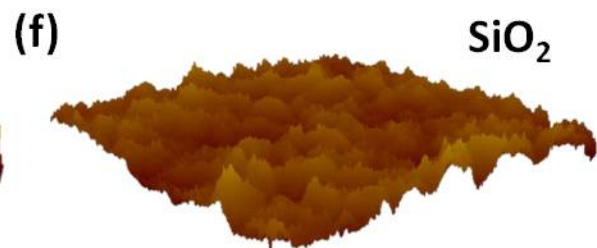
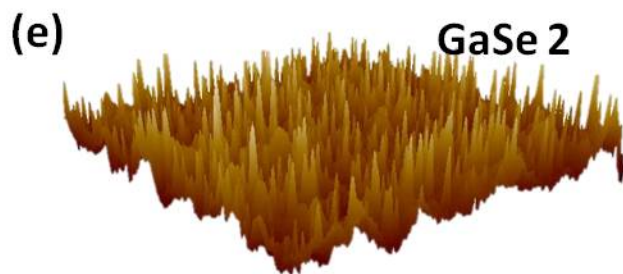
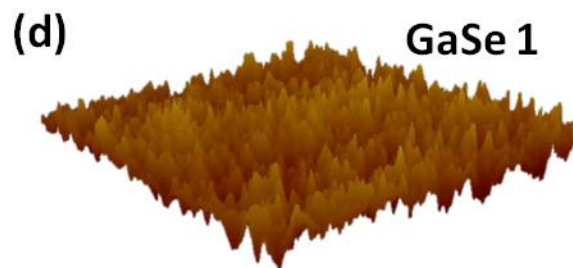
- 22 B. Sachs, L. Britnell, T. O. Wehling, A. Eckmann, R. Jalil, B. D. Belle, A. I. Lichtenstein, M. I. Katnelson, and K. S. Novoselov, *Appl. Phys. Lett.*, **103**, 251607 (2013).
- 23 S. Ross, and A. Sussman, *J. Phys. Chem.* **59**, 889-892 (1955).
- 24 C. F. Higgs, C. A. Heshmat, and H. Heshmat, *J. Tribol.*, **121**, 625-630 (1999).
- 25 M. T. Lavik, T. M. Medved, and G. D. Moore, *ASLE Trans.*, **11**, 44 (1968).
- 26 A. M. Goossens, V. E. Calado, A. Barreiro, K. Watanabe, T. Taniguchi, and L. M. K. Vandersypen, *Appl. Phys. Lett.*, **100**, 073110 (2012).
- 27 M. Yamamoto, T. L. Einstein, M. S. Fuhrer, and W. Cullen, *ACS Nano*, **6**, 9 (2012).
- 28 L. A. Ponomarenko, R. Yang, T. M. Mohiuddin, M. I. Katnelson, K. S. Novoselov, S. V. Morozov, A. A. Zhukov, F. Schedin, E. W. Hill, and A. K. Geim, *Phys. Rev. Lett.*, **102**, 206603 (2009).
- 29 H. Wang, Y. Wu, C. Cong, J. Shang, and T. Yu, *ACS Nano*, **4**, 12 (2010).
- 30 W. Kim, A. Javey, O. Vermesh, Q. Wang, Y. Li, and H. Dai, *Nano Lett.* **3**, 193-198 (2003).
- 31 S. Larentis, J. R. Tolsma, B. Fallahazad, D. C. Dillen, K. Kim, A. H. MacDonald, and E. Tutuc, *Nano Lett.* **14**, 2039–2045 (2014).
- 32 A. V. Kertinin, Y. Cao, J. S. Tu, G. L. Yu, R. Jalil, K. S. Novoselov, S. J. Haigh, A. Gholinia, A. Mishchenko, M. Lozada, T. Georgiou, C. Woods, F. Withers, P. Blake, G. Eda, A. Wirsig, C. Hucho, K. Watanabe, T. Taniguchi, A. K. Geim, and R. V. Gorbachev, arXiv: 1403.5225.

Figure Captions

Fig. 1. Typical AFM scanning images of (a) BN, (b) WS₂, (c) MoS₂, (d-e) GaSe immediately after exfoliation and 1 day after exfoliation and (f) SiO₂. Height scale of the AFM image is 0-3 nm and scanning dimension is 1 μm x 1 μm. (g-h) Height histogram and rms analysis of the images are shown in panels (a-f) respectively. (i) A completed graphene Hall bar device on WS₂ substrate.

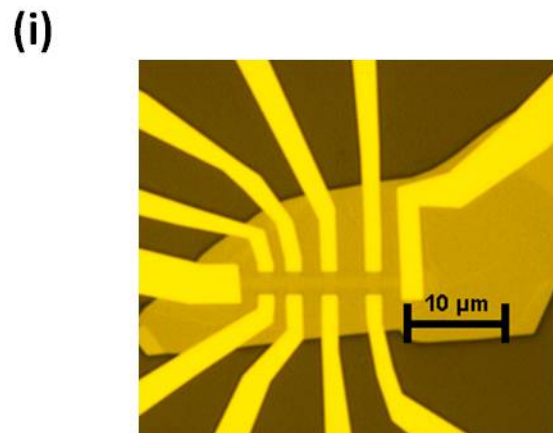
Fig. 2. (a) Resistivity and conductivity of graphene on WS₂ substrate as a function of V_{BG} at RT. Inset- V_{BG} dependence graphene resistivity on BN substrate at 5K. (b) Resistivity and conductivity of graphene on MoS₂ substrate at RT.

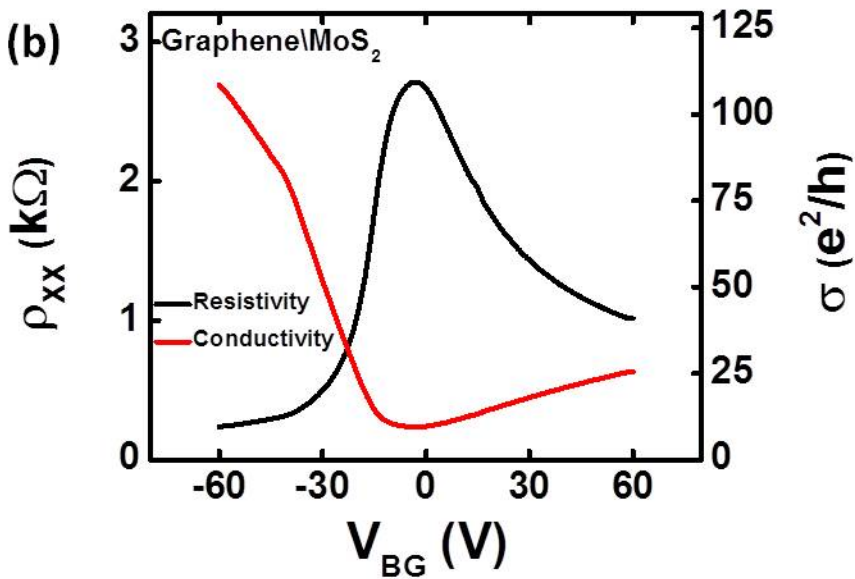
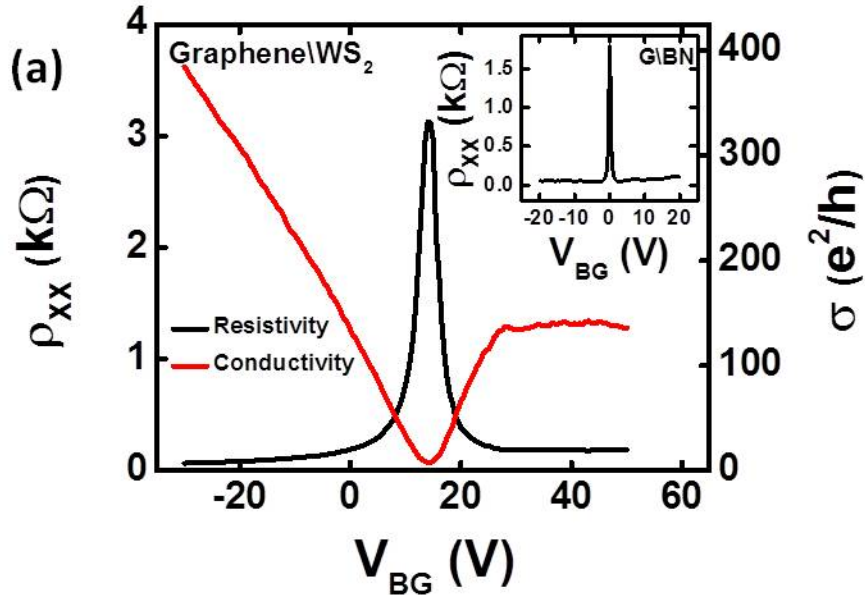
Fig. 3. (a) Resistivity and conductivity of graphene on GaSe substrate as a function of V_{BG}. (b) Resistivity of graphene as a function of different V_{BG} ranges. Black and red arrows represent the sweep directions from negative to positive and positive to negative, respectively. (c) Dark field images of GaSe crystal just after exfoliation and as a function of time.

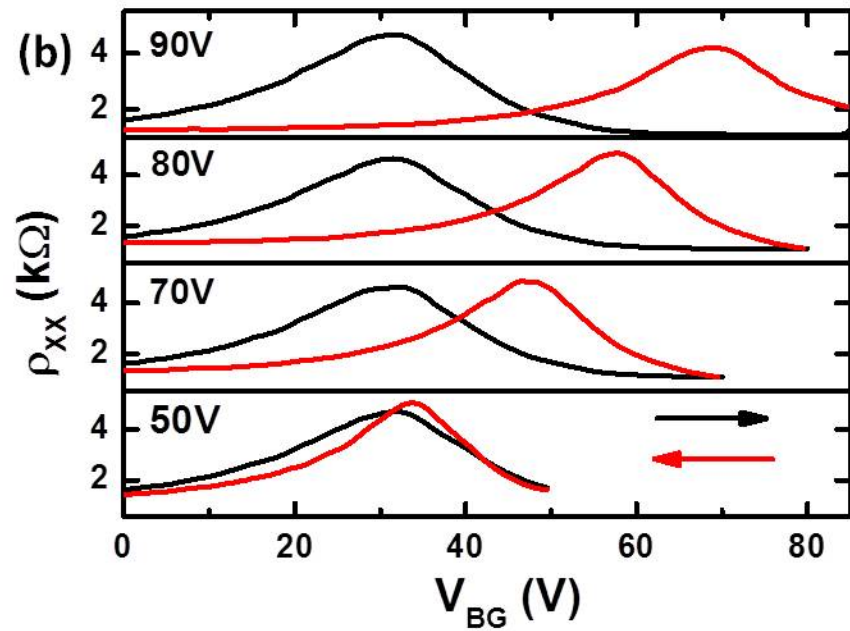
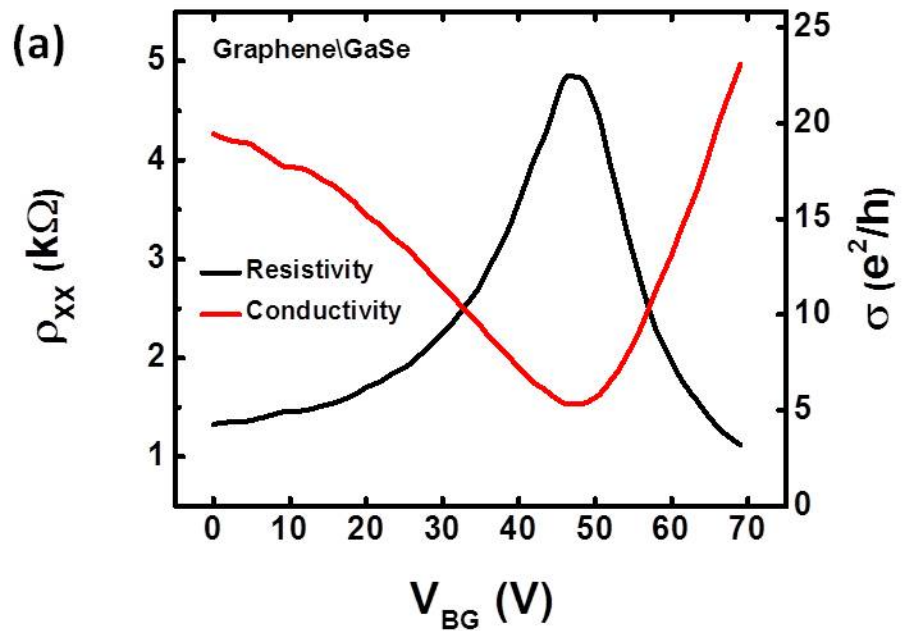


(h)

Substrate	Roughness (nm)
BN	0.06nm
WS ₂	0.08nm
MoS ₂	0.09nm
GaSe-1	0.12nm
GaSe-2	0.185nm
SiO ₂	0.17nm







(c)

